Mechanistic Insights from the Binding of Substrate and Carbocation Intermediate Analogues to Aristolochene Synthase

Mengbin Chen[†], **Naeemah Al-lami**[‡], **Marine Janvier**[‡], **Edward L. D'Antonio**[†], **Juan A. Faraldos**[‡], **David E. Cane**[§], and **Rudolf K. Allemann**[‡], and **David W. Christianson**[†,*]

[†]Roy and Diana Vagelos Laboratories, Department of Chemistry, University of Pennsylvania, Philadelphia, Pennsylvania, 19104-6323 USA

[‡]School of Chemistry, Cardiff University, Park Place, Cardiff CF10 3AT, Wales, United Kingdom

[§]Department of Chemistry, Box H, Brown University, Providence, RI 02912-9108 USA.

Abstract

Aristolochene synthase, a metal-dependent sesquiterpene cyclase from *Aspergillus terreus*, catalyzes the ionization-dependent cyclization of farnesyl diphosphate (FPP) to form the bicyclic eremophilane (+)-aristolochene with perfect structural and stereochemical precision. Here, we report the X-ray crystal structure of aristolochene synthase complexed with three Mg^{2+} ions and the unreactive substrate analogue farnesyl-*S*-thiolodiphosphate (FSPP), showing that the substrate diphosphate group is anchored by metal coordination and hydrogen bond interactions identical to those previously observed in the complex with three Mg^{2+} ions and inorganic pyrophosphate (PP_i). Moreover, the binding conformation of FSPP directly mimics that expected for productively bound FPP, with the exception of the precise alignment of the C-S bond with regard to the C10-C11 π system that would be required for C1-C10 bond formation in the first step of catalysis. We also report crystal structures of aristolochene synthase complexed with $Mg^{2+}{}_3$-PP_i and ammonium or iminium analogues of bicyclic carbocation intermediates proposed for the natural cyclization cascade. Various binding orientations are observed for these bicyclic analogues, and these orientations appear to be driven by favorable electrostatic interactions between the positively charged ammonium group of the analogue and the negatively charged PP_i anion. Surprisingly, the active site is sufficiently flexible to accommodate analogues with partially or completely incorrect stereochemistry. Although this permissiveness in binding is unanticipated, based on the stereochemical precision of catalysis that leads exclusively to the (+)-aristolochene stereoisomer, it suggests the ability of the active site to enable controlled reorientation of intermediates during the cyclization cascade. Taken together, these structures illuminate important aspects of the catalytic mechanism.

Terpenoids, including steroids and carotenoids, comprise the largest class of natural products, with more than 70,000 members identified to date (Dictionary of Natural Products: http://dnp.chemnetbase.com). Remarkably, the structural and stereochemical complexity of these organic molecules is rooted in diverse biosynthetic pathways involving simple 5-carbon isoprenoid precursors. For example, dimethylallyl diphosphate and two molecules of

isopentenyl diphosphate can be coupled together in head-to-tail fashion to generate the C_{15}-isoprenoid farnesyl diphosphate,[1,2] which can then be converted into myriad cyclic hydrocarbon products through multi-step reactions catalyzed by sesquiterpene synthases.[3-11]

Class I terpenoid cyclases share a common α-helical fold and utilize a trinuclear metal ion cluster (usually Mg^{2+}, sometimes Mn^{2+} or Co^{2+}) to trigger the departure of the pyrophosphate (PP_i)[a] leaving group. This generates a highly reactive allylic cation that reacts with one of the remaining π bonds of the substrate, thereby initiating a cyclization sequence typically proceeding through multiple carbocation intermediates. The binding of three Mg^{2+} ions and substrate induces protein conformational changes that enclose the active site, as first observed in the structure of trichodiene synthase complexed with Mg^{2+}_3-PP_i,[12] which establishes a cyclization-competent substrate conformation and protects carbocation intermediates from premature quenching by solvent. The specific sequence of carbon-carbon bond forming reactions is governed by the conformational control that the enzyme exerts over the substrate and the stabilization of carbocation intermediates. Ultimately, the cyclization cascade is terminated by deprotonation or addition of water to the final carbocation intermediate. Intriguingly, while many cyclases are high-fidelity enzymes that precisely chaperone successive carbocation intermediates to form a single product, others are more promiscuous in that they generate a mixture of products.

Aspergillus terreus aristolochene synthase (ATAS) catalyzes the cyclization of farnesyl diphosphate (FPP) to form the bicyclic eremophilane (+)-aristolochene (Figure 1), which is the hydrocarbon parent of several fungal toxins such as gigantenone, bipolaroxin, and PR-toxin.[13] Unlike its counterpart in *Penicillium roqueforti* that produces a mixture of products, ATAS is a high fidelity enzyme that generates (+)-aristolochene exclusively.[14] To date, no crystal structures of *Penicillium roqueforti* aristolochene synthase or ATAS complexed with analogues of substrate or carbocation intermediates have been reported in which the active site is locked in the fully closed, active conformation by three Mg^{2+} ions. Here, we report the structure of the ATAS-Mg^{2+}_3 complex with the unreactive substrate analogue farnesyl thiolodiphosphate (FSPP), as well as the first structures of ATAS-Mg^{2+}_3 complexes with ammonium and iminium aza-analogues of possible carbocation intermediates in the cyclization cascade (Figure 1). While carbocation intermediates are of course too short-lived to be studied in their enzyme complexes by typical X-ray crystallographic methods, the use of cationic aza-analogues enables the study of molecular strategies for stabilizing and manipulating the transient carbocation intermediates that they mimic.[15-17] Additionally, the binding of aza-analogues with unusual stereochemistries provides insight on the structural basis of fidelity in the cyclization cascade that exclusively yields (+)-aristolochene.

Materials and Methods

Aza-analogues of carbocation intermediates

The syntheses of (4a*S*,7*S*)-4a-methyl-7-(prop-1-en-2-yl)-2,3,4,4a,5,6,7,8-octahydroquinolin-1-ium (**1**) and (4a*S*,7*S*)-1,4a dimethyl-7-(prop-1-en-2-yl)decahydroquinolin-1-ium (**2**) have been previously reported.[18,19] The syntheses of (3*R*, 6*R*,9a*R*)-6,9a-dimethyl-3-(prop-1-en-2-yl)decahydroquinolizin-5-ium (**3**) and (1*S*,8*S*, 9a*R*)-1,9a-dimethyl-8-(prop-1-en-2-yl)decahydroquinolizin-5-ium (**4**) were accomplished in 6 and 8 steps, respectively, starting from the known keto ester (*S*)-methyl-6-oxo-3-(prop-1-en-2-yl)heptanoate, which was obtained by degradation of (–)-limonene.[20-22] The synthesis

---

of **3** features a modified Curtius rearrangement[23] that gives rise to the 3,6-dialkylated cyclic imine (*R*)-6-methyl-3-(prop-1-en-2-yl)-2,3,4,5-tetrahydropyridine after acid-promoted cyclization.[24] The latter was easily converted to the final (3*R*,6*R*,9a*R*)-trialkyl substituted quinolizidine **3** essentially as described by De Kimpe.[25] This protocol generates an equal amount of the (3*R*,6*S*,9a*S*)-diastereomer of **3**. Starting from the same (*S*)-configured keto ester, imine **4** was prepared via a Beckmann rearrangement[26,27] that provided after cyclization[27] the enantiopure lactam (*S*)-4-(prop-1-en-2-yl)piperidin-2-one. This lactam was then converted to the final quinolizidine **4** via a tandem aza-Robinson annulation/Michael alkylation/Wolff-Kishner reduction that installed the syn vicinal methyl groups of **4** with excellent stereospecificity.[28-30] An identical synthetic protocol was repeated from (+)-limonene to give (1*R*,8*R*,9a*S*)-1,9a-dimethyl-8-(prop-1-en-2-yl)decahydroquinolizin-5-ium (**5**), the enantiomer of quinolizidine **4**. The absolute configuration of amines **3**, **4**, and **5** was determined using a combination of 1D and 2D NMR experiments and confirmed by X-ray crystal structure determinations of the perchlorate salts of **3**, **4** and **5**. Full details of the syntheses of amines **3-5** will be published separately.

Preparation of recombinant ATAS

To minimize molecular disorder and simplify enzyme purification, a new truncation variant of ATAS was prepared in which the first 12 residues at the N terminus were deleted and replaced by a hexahistidine tag using PCR mutagenesis. This was achieved in two separate steps. First, to prepare the deletion variant, the forward and reverse primers for the deletion were as follows: 5'–GTT TAA CTT TAA GAA GGA GAT ATA CAT ATG CTT GAG CCA CCC CCC TCT ACG TTC–3', and 5'–GAA CGT AGA GGG GGG TGG CTC AAG CAT ATG TAT ATC TCC TTC TTA AAG TTA AAC–3'. Plasmids were transformed into *Escherichia coli* XL1-Blue cells (Novagen) and amplified. They were purified using miniprep kits and the deletion was confirmed by DNA sequencing. In the second step, the His$_6$ tag was spliced between M1 and L14 of the deletion variant to generate the new truncation variant designated His$_6$-Δ12-ATAS. The corresponding primers were: 5'–GTT TAA CTT TAA GAA GGA GAT ATA CAT ATG CAT CAT CAC CAT CAC CAT CTT GAG CCA CCC CCC TCT ACG TTC–3', and 5'–CAA ATT GAA ATT CTT CCT CTA TAT GTA TAC GTA GTA GTG GTA GTG GTA GAA CTC GGT GGG GGG AGA TGC AAG–3'. Plasmids of His$_6$-Δ12 ATAS were prepared and purified as described above.

Escherichia coli BL21(DE3)-pLysS cells (Stratagene, Agilent) carrying the cDNA for His$_6$-Δ12 ATAS (henceforth designated simply "ATAS") were inoculated in 6×5 mL Luria Bertani (LB) medium containing 100 μg/mL ampicillin and grown for 6 hrs at 37 °C with shaking (250 rpm). Each 5 mL culture was used to inoculate 6×1L LB medium containing 100 μg/mL ampicillin. When OD$_{600}$ reached 1.0, the temperature was adjusted to 22 °C, and 1 mM isopropyl β-D-1-thiogalactopyranoside was added to induce protein synthesis. The expression lasted for 7.5 hrs before the cells were pelleted and stored at −80 °C for further use.

The cell pellet was thawed and suspended in 50 mL of Talon (QIAGEN) wash buffer [50 mM 3-(*N*-morpholino)-propanesulfonic acid (MOPS) (pH 7.0), 300 mM NaCl, 2 mM β-mercaptoethanol (BME), 10% glycerol]. After sonication, the cell lysate was centrifuged at 15,000 rpm and the supernatant loaded onto a pre equilibrated Talon column at a flow rate of 2 mL/min. Enzyme was eluted with a 0-150 mM imidazole gradient in Talon wash buffer. The most active fractions were combined and dialyzed against HiTrap Q HP wash buffer [20 mM 2 morpholinoethanesulfonic acid (MES) (pH 6.5), 5mM ethylenediaminetetraacetic acid (EDTA), 5 mM BME, 10% glycerol] (GE Healthcare Life Sciences). After loading on a HiTrap Q HP column (15 mL), enzyme was eluted with a 0-500 mM sodium chloride gradient in HiTrap Q HP wash buffer. Selected fractions were pooled, concentrated, and

further purified in 25 mM MES (pH 6.5), 2 mM $MgCl_2$, 150 mM NaCl, 4 mM BME using a HiLoad 26/60 Superdex column (GE Healthcare Life Sciences). The final ATAS sample was 98% pure as indicated by SDS-PAGE and was concentrated to 10 mg/mL.

Crystal structure determinations

Crystals of ATAS-inhibitor complexes were prepared by cocrystallization in hanging drops through the vapor diffusion method at 4 °C. Briefly, a 3 µL drop of protein solution [10 mg/ mL ATAS, 20 mM MES (pH 6.5), 1.9 mM $MgCl_2$, 120 mM NaCl, 3 mM BME, 1.6 mM sodium pyrophosphate, 1.5 mM inhibitor] was added to a 3 µL drop of precipitant solution and equilibrated against a 500 µL reservoir of precipitant solution. Different precipitant solutions were used for the crystallization of different ATAS-inhibitor complexes as follows: for FSPP (Echelon Biosciences), the precipitant solution was 200 mM magnesium acetate, 17% polyethylene glycol (PEG) 3350; for **1**, the precipitant solution was 100 mM 4-(2-hydroxyethyl)-1-piperazineethanesulfonic acid (HEPES) (pH 7.7), 200 mM $MgCl_2$, 23% (w/v) PEG 3350; for **2**, the precipitant solution was 100 mM Bis-Tris (pH 7.0), 200 mM Li_2SO_4, and 27% (w/v) PEG 3350; for **3**, the precipitant solution was 100 mM magnesium formate, 12% PEG 3350; for **4**, the precipitant solution was 2% Tacsimate (pH 6.0), 100 mM Bis Tris (pH 7.0), 16% (w/v) PEG 3350; for **5**, the precipitant solution was 200 mM sodium malonate (pH 7.0), 15% (w/v) PEG 3350. Crystals generally appeared within 1 week and grew to maximum size within 3-4 weeks. Crystals were gradually transferred to cryoprotectant solution (20 % (v/v) glycerol in mother liquor) and flash-cooled in liquid nitrogen.

X-ray diffraction data were collected at beamlines X25 and X29A of the National Synchrotron Light Source at Brookhaven National Laboratory, and were indexed, integrated, and scaled using HKL2000.[31] Criteria for determining the resolution cut-off for each data set included $R_{merge} < 0.140$ and $I/\sigma > 1.5$ for outer shell data. For the ATAS-**2** complex at 2.4 Å resolution, we had collected slightly higher resolution data sets in different experiments, but we were not able to index these data sets. In the data set that we were able to index, we were limited to 2.4 Å resolution data due to the geometry of the X-ray diffraction experiment. The R_{pim} value was calculated using phenix.merging_statistics in the PHENIX GUI.[32] Molecular replacement was performed with Phaser for Molecular Replacement in the CCP4i package,[33] using a monomer of the previous determined structure of ATAS[34] as a search probe for rotation function and translation function calculations. All crystals formed in a new space group compared with that of the previously reported crystals of full-length ATAS[34,35] and belonged to space group $P3_121$ with four monomers in the asymmetric unit as a dimer of dimers. The quaternary structure of this dimer of dimers is similar but not identical to that reported for full-length ATAS crystallized in space group $P2_1$: one dimer is rotated relative to the second dimer by approximately 30°. Refinement and manual model adjustment were performed with PHENIX and COOT, respectively.[36,37] The disordered N terminus M1-H7 and C-terminus V312-D314 were excluded in most final models. Refinement statistics are recorded in Table 1. MolProbity was used to validate all structures.[38]

Results

ATAS-FSPP complex

The ATAS-FSPP complex crystallizes with four monomers (designated A-D) in the asymmetric unit as a dimer of dimers, and this arrangement is observed for all complexes prepared with the new ATAS construct utilized in the current study. Roughly similar quaternary structure is observed in previously-determined crystal structures of full-length ATAS in a different space group.[34] Significant conformational changes are triggered by the

binding of FSPP and three Mg^{2+} ions in the active site, and the root-mean-square (r.m.s.) deviation is 1.2 Å for 241 $C\alpha$ atoms between the ATAS-FSPP complex and unliganded ATAS (Figure 2).[34] These structural changes include the ordering of the C-terminal end of helix H and the H-α-1 loop (this helps to "cap" the active site), a short coil-helix transition within the F-G1 loop, and the introduction of a small kink in helix I. These structural changes are essentially identical to those observed in the ATAS-Mg^{2+}_3-PP_i complex[34] and appear to be driven by protein and substrate coordination interactions with the trinuclear magnesium cluster.

A simulated annealing omit map of the ATAS-FSPP complex is shown in Figure 3a. The α-helices surrounding the active site shift ca.1.5 Å inward to facilitate van der Waals interactions with the isoprenoid chains of FSPP, and the S225-I234 segment, which was disordered in the unliganded enzyme, becomes ordered and caps the top of the active site. The side chains of E221, N213, and D84 undergo conformational changes to enable Mg^{2+} coordination, and the side chains of R169, N213, K220, R308, and Y309 move to donate hydrogen bonds to the diphosphate group of FSPP. Comparison with the structure of the ATAS-Mg^{2+}_3-PP_i complex[34] shows that the geometry of metal coordination and hydrogen bond interactions with the diphosphate group is maintained regardless of whether or not the diphosphate group is covalently bonded to an isoprenoid (Figure 3b). Deeper in the hydrophobic cavity, it appears that the side chains of V57, L77, and L80 flip to better encase the isoprenoid chain of FSPP (admittedly, these conformational changes could also be the result of refinement with higher resolution diffraction data). The structure of the ATAS-FSPP complex is essentially identical in monomers A-C; slight differences are observed in monomer D, presumably due to the somewhat noisy electron density that characterizes FSPP.

The intermolecular interactions of the diphosphate group of FSPP appear to indirectly influence the isoprenoid chain conformation. The previously determined structure of ATAS complexed with 2-fluorofarnesyl diphosphate revealed the binding of only one Mg^{2+} ion to an incomplete closed active site.[35] Consequently, the isoprenoid conformation and orientation of 2-fluorofarnesyl diphosphate is "flipped" relative to that now observed for FSPP. Therefore, we conclude that a full complement of 3 Mg^{2+} ions is required to achieve complete active site closure,[10] which in turn is required to achieve a catalytically-productive substrate conformation.

In the ATAS-FSPP complex, the distance between C10 and C1 of FSPP is 4.6 Å (monomer A); additionally, the orientation of the C1-S bond with respect to the π system at C10 would not support the C1-C10 bond forming reaction that initiates the cyclization cascade. Since the isoprenoid chain of FSPP is otherwise bound with a productive conformation, however, with the C14 and C15 methyl groups and the terminal isopropylidene group adopting a conformation that would lead to the formation of (S)-(–)-germacrene A as outlined in Figure 1, all that would be necessary for a fully productive conformation would be a ~90° rotation about the C3-C2-C1-S dihedral angle to align the C1-S bond for backside attack by the π system at C10, which would give rise to the observed inversion of configuration at C1.[39]

Studies with isotopically labeled FPP have demonstrated that the initial cyclization reaction forming (S)-(–)-germacrene A requires regiospecific deprotonation of the C13 cis-methyl group of the germacryl cation as shown in Figure 1.[40] Although the phenolic side chain of Y61 is 3.7 Å away from the C13 cis-methyl group of FSPP (monomer A), mutagenesis studies of this residue show that while it is required for optimal catalytic activity,[41] it is not obligatory for the generation of (+)-aristolochene.[14] Thus, Y61 cannot be a catalytically required general base. The C13 cis-methyl group is only 4.0 Å from the thiophosphate sulfur atom of FSPP, however, suggesting the possibility that the corresponding oxygen atom of

the diphosphate group of FPP could serve as the general base responsible for the regiospecific proton elimination from the intermediate germacryl cation intermediate shown in Figure 1.

It is interesting to note that a water molecule, labeled "w" in Figure 3, is trapped in the upper active site. This water molecule is fixed in place by hydrogen bonds with N213, N299, and S303. The C13 cis-methyl group of FSPP is 3.9 Å away from water molecule "w" while the C12 trans-methyl group of FSPP is 3.0 Å away (monomer A). Based on the observed binding conformation of FSPP, water molecule "w" is unlikely to mediate the regiospecific deprotonation of the C13 cis-methyl group.

Finally, the steric bulk of aromatic amino acids often defines in large part the active site contour of a terpenoid cyclase, and this is the case for ATAS. Active site aromatic residues thus play an important role in chaperoning the binding conformation of the flexible isoprenoid substrate. The C1-C4 isoprenoid unit of FSPP makes van der Waals contacts with the side chain of F147, while the distal C9-C12 isoprenoid unit is nestled within a shallow crevice formed by the side chains of Y61, F81, and W302. Aromatic residues may also provide electrostatic stabilization of carbocation intermediates and their flanking transition states through cation-π interactions.[42-44]

ATAS-1 complex

Even though its lacks an N-methyl substituent, iminium cation **1** mimics the eudesmane cation intermediate of the ATAS reaction, presuming that the sp^2-hybridized iminium nitrogen is protonated (pKa ≈ 7-8) and positively charged (Figure 1).[18,19] The simulated annealing omit map of this complex (Figure 4a) reveals that the Mg^{2+}_3 cluster and PP_i group bind with full occupancy and make similar interactions to those observed in the ATAS-FSPP complex, thereby ensuring a fully closed active site conformation. The structure of the ATAS-**1** complex is essentially identical in monomers A-C; slight differences are observed in monomer D, possibly due to somewhat noisy electron density. In general, active site residues adopt nearly identical conformations in the ATAS-**1** and ATAS-FSPP complexes. Intriguingly, however, the orientation of **1** is flipped ~180° relative to that of FSPP, such that the isopropylidene group is sandwiched between F81 and F147 rather than in the shallow crevice formed by the side chains of Y61, F81, and W302 (Figure 4b). Accordingly, the iminium NH group of **1** donates two hydrogen bonds to the PP_i group. Thus, favorable electrostatic and hydrogen bond interactions appear to play a dominant role in governing the binding orientation of **1**.

Trapped water molecule "w" observed in the ATAS-FSPP complex is also present in the ATAS-**1** complex and it makes a similar array of hydrogen bond interactions with N213, N299, and S303. Presuming that water molecule "w" remains bound upon the binding of the actual substrate FPP, hydrogen bond interactions presumably restrain water molecule "w" so that it cannot react with any carbocation intermediates since ATAS does not generate any hydroxylated products.[14] Accordingly, this water molecule appears to be an integral part of the active site contour and inert with regard to the chemistry of catalysis.

ATAS-2 complex

The simulated annealing omit map of this complex (Figure 5a) reveals that the Mg^{2+}_3 cluster, the PP_i anion, and tertiary amino cation **2** bind with full occupancy, and the active site adopts a fully closed conformation. Although the resolution of this structure (2.4 Å) is the lowest of the structures described in the current work, the electron density envelope outlining **2** is reasonably well-defined in all four monomers and the structure of the ATAS-**2** complex is essentially identical in all four monomers.

Tertiary amino cation **2** mimics the eudesmane cation intermediate and binds with an orientation somewhat similar to that of **1**, in that the isopropylidene group lies between F81 and F147. The positively charged amino group of **2** donates a hydrogen bond to the PP$_i$ group, although it is tilted slightly downward and shifted toward F147 and F81 relative to the position of **1** to avoid a steric clash between the *N*-methyl substituent and the PP$_i$ group. Consequently, the side chain of L77 is flipped to accommodate the isopropylidene group of **2**. The trapped water molecule "w" is present, but it does not make any close contacts with **2**. A superposition of the ATAS-**1** and ATAS-**2** complexes is shown in Figure 5b.

ATAS-3 complex

The simulated annealing omit map of this complex (Figure 6a) reveals that the Mg$^{2+}_3$ cluster, PP$_i$ anion, and **3** bind with full occupancy in a fully closed active site. The structure of the ATAS-**3** complex is essentially identical in all four monomers. Compound **3** partially mimics the possible carbocation intermediate that would be formed in a stepwise mechanism in which the eudesmane cation undergoes a 1,2-hydride transfer to form a tertiary carbocation at the ring-fusion carbon (Figure 1). However, **3** is an imperfect mimic, because the stereochemistry at the C3 atom is *R* instead of *S*, the protonated amino nitrogen is sp^3-hybridized rather than sp^2-hybridized, and the analogue adopts a conformation comparable to that of a cis-decalin. Even so, the binding orientation of **3** is somewhat reminiscent of that of FSPP, in that the isopropylidene group is nestled with the cavity formed by the side chains of Y61, F81, and W302 (Figure 6b). Although the conformations of surrounding residues are identical to those observed in previous structures, F81 moves slightly toward the bottom of the cleft to accommodate **3**. Notably, there is an additional water molecule, labeled "ww", that hydrogen bonds with a Mg$^{2+}_C$-bound water molecule, donates a hydrogen bond to the PP$_i$ group, and accepts a hydrogen bond from the protonated amino group of **3**.

Despite the fact that **3** is an imperfect analogue of a possible carbocation intermediate in the ATAS reaction, it is interesting to note that the methylene group corresponding to that which undergoes stereospecific deprotonation of the H-8$_{si}$ atom is oriented toward the PP$_i$ anion. This suggests the possibility that the PP$_i$ anion could serve as a general base that removes the H-8$_{si}$ proton[40] in the cyclization cascade leading to (+)-aristolochene formation as shown in Figure 1.

ATAS-4 complex

The simulated annealing omit map of this complex (Figure 7a) reveals that the Mg$^{2+}_3$ cluster, PP$_i$ anion, and **4** bind with full occupancy, ensuring a fully closed active site conformation. The structure of the ATAS-**4** complex is essentially identical in monomers A–C; slight differences are observed in monomer D, presumably due to the relatively poor electron density that characterizes **4**. Tertiary amino cation **4** mimics the final carbocation intermediate proposed in the stepwise mechanism leading to the formation of (+)-aristolochene. Although the amino nitrogen bears a positive charge and all stereocenters are correctly constructed, the sp^3-hybridization of the cationic tertiary amino group makes it an imperfect mimic of the planar sp^2-hybridized tertiary carbocation shown in Figure 1. The amino nitrogen of **4** faces the PP$_i$ group, and van der Waals interactions occur between the ring carbon atoms of **4** and the PP$_i$ group (Figure 7a). The isopropylidene group of **4** is nestled in the aromatic cleft formed by Y61, F81, and W302. This is the same general location occupied by the terminal isoprenoid unit of FSPP, as shown in the superposition in Figure 7b. If this orientation were adopted by the final carbocation intermediate in catalysis, it is interesting to note that the C8 methylene group is oriented toward the PP$_i$ anion. This further supports the possibility that the PP$_i$ anion could serve as a general base for the stereospecific deprotonation of the H-8$_{si}$ atom in the cyclization of FPP to (+)-aristolochene.

ATAS-5 Complex

In order to probe stereochemical discrimination in the active site of ATAS, we prepared the complex with tertiary ammonium cation **5**. This analogue has opposite stereochemistry at all stereocenters relative to **4**, including the stereochemistry at the protonated tertiary amino group. The stereochemistry of **5** is therefore inconsistent with that of any structure encountered in the natural ATAS mechanism shown in Figure 1. Despite this fact, **5** is readily accommodated in the active site of ATAS, which is stabilized in the fully closed conformation by Mg^{2+}_3-PP_i bound with full occupancy (Figure 8a). The structure of the ATAS-**5** complex is essentially identical in monomers A-D, even though the electron density of **5** in monomer D is somewhat noisy. To avoid a steric clash with the isopropylidene group, Y61 rotates ~90° relative to its observed conformation in the ATAS-**4** complex, but the conformations of other active site residues are essentially identical to those observed in the ATAS-**4** complex. As in other complexes, trapped water molecule "w" hydrogen bonds with N213, N299, and S303; the additional trapped water molecule, "ww" is also observed and is stabilized by hydrogen bond interactions with the PP_i group, a Mg^{2+}_C-bound water molecule, and the amino group of **5**. A superposition comparing the binding modes of correct stereoisomer **4** and incorrect stereoisomer **5** complexed with ATAS is shown in Figure 8b.

Discussion

Aromatic triad Y61, F81, and F147 enables cation-π stabilization and contributes to the template for FPP cyclization

The structures of the several bicyclic aza analogues of carbocation intermediates bound in the active site of ATAS demonstrate the feasibility of cation stabilization through charge-quadrupole or cation-π interactions,[42,43] as originally suggested in the first reported structures of terpenoid cyclases.[45-47] While different positions and orientations are observed for each, analogues **1-4** bind in a region that is encircled by the faces of three aromatic residues: Y61, F81, and F147 (Figures 4-7). Due to the conformational change of Y61 that accommodates the binding of analogue **5**, which has "incorrect" stereocenters, the edge of this residue rather than its face is oriented toward the active site cavity (Figure 8). Nevertheless, the binding of aza analogues **1-4**, which better mimic carbocation intermediates in the ATAS reaction, suggests that Y61, F81, and F147 are ideally positioned to stabilize carbocation intermediates and their intervening transition states in the ATAS reaction.

Residues Y61, F81, and F147 are conserved in the closely related aristolochene synthase from *P. roqueforti* (PRAS) as Y92, F112, and F178, consistent with a conserved functional role for these aromatic residues. Interestingly, Y92F PRAS exhibits lower catalytic activity[14,41] but nevertheless retains the ability to generate aristolochene;[14] the Y92V, Y92C, and Y92A mutations similarly exhibit compromised catalytic activity but also generate (*E*)-β-farnesene, demonstrating that the bulky tyrosine side chain is part of the template that enforces the cyclization of FPP to form aristolochene.[48,49] A template function for the aromatic triad is consistent with the structure of the ATAS-FSPP complex (Figure 3), in which Y61, F81, and F147 make significant van der Waals contacts with the flexible isoprenoid group of the substrate analogue, thereby enforcing its bound conformation.

Structural studies of the unrelated bacterial sesquiterpene cyclase epi-isozizaene synthase have also shown that three aromatic residues (F95, F96, and F198) encircle the active site and make cation-π interactions with the benzyltriethylammonium cation;[16] the bacterial sesquiterpene cyclase pentalenene synthase also contains three aromatic residues (F76, F77, and Y146) oriented so as to enable cation-π interactions in the active site.[45] Alternatively,

sesquiterpene cyclase active sites can be defined by the faces of only two aromatic residues capable of engaging in cation-π interactions, such as those of 5-epi-aristolochene synthase (W273 and Y527),[46] trichodiene synthase (Y93 and F157),[12] and δ-cadinene synthase (W279 and Y527).[50] Thus, a working hypothesis is that a sesquiterpene cyclase active site can be encircled by a triad of aromatic residues with general primary structure $(F,Y)X_{1-20}FX_{70-100}(F,Y)$; if not, then it contains two aromatic residues quite distant from one another in the protein primary structure with their ring faces oriented toward the active site.

Charge-charge interactions with the PPᵢ anion appear to govern the orientation of cationic aza-analogues

It is notable that bicyclic aza analogues **1-4** bind with two general orientations. In one orientation, the branched isopropylidene group is nestled between F81 and F147 (analogues **1** and **2**); in the other orientation, the isopropylidene group is oriented toward Y61 (analogues **3** and **4**). In the ATAS-FSPP complex, the isopropylidene C12 and C13 atoms are similarly oriented toward Y61 (Figure 1). Although it is unlikely that the carbocation intermediates in the ATAS reaction exhibit exceptional mobility during catalysis that would facilitate lengthwise flipping of the bicyclic ring system, the ability of ATAS to accommodate multiple conformations of the aza analogues suggests the intriguing possibility that the transiently generated, uncharged germacrene A intermediate may undergo a reorientation within the active site cavity so as to present the 6,7-double bond to the co-generated pyrophosphoric acid, allowing protonation at C6, followed by transannular cyclization, rearrangement, and final deprotonation of H-8$_{si}$ by the appositely located PPᵢ anion. In principle, the requisite reorientation of the germacrene could take place either by a ~120° rotation about an axis passing through the average plane of the germacrene A ring, or by a ~180° rotation about an axis passing through C5 and C10. Since the PPᵢ ion appears to be firmly anchored by the surrounding network of ion-metal, oxyanion-cation, and hydrogen bond interactions, reorientation of the germacrene A intermediate would allow the pyrophosphate to access both C6 and C8 in order to mediate the key protonation and eventual deprotonation steps at these centers with the observed stereochemistry.

Interestingly, in each enzyme-inhibitor complex, the cationic ammonium or iminium group is oriented toward the PPᵢ anion, so the binding orientation of each aza analogue appears to be governed largely by favorable charge-charge interactions with the PPᵢ anion and not just cation-π interactions with aromatic residues. Positively-charged ammonium groups of aza analogues **1** and **2** donate hydrogen bonds directly to the PPᵢ anion, and aza analogues **3** (and **5**) donate hydrogen bonds to water molecule "ww", which in turn donates a hydrogen bond to the PPᵢ anion. Aza analogue **4**, while not hydrogen bonding to the PPᵢ anion, is oriented so that the positively-charged amino group is near the PPᵢ anion. Presumably, the thermodynamically favored binding position and orientation of the aza analogue in the enzyme active site is attained as enzyme and inhibitor equilibrate in the cocrystallization experiment. Thus, the observation of two general binding orientations for these analogues is likely to be an artifact of favorable charge-charge interactions between the aza analogues and the PPᵢ anion.

Which orientation, then, corresponds to the productive orientation of catalysis? We hypothesize that the catalytically productive orientation is that which orients the isopropylidene group toward Y61, since this orientation better corresponds to that observed for the binding of the substrate analogue FSPP. The binding orientation and conformation of FSPP is not subject to direction by PPᵢ anion-cation interactions, and FSPP is bound with a nearly-productive conformation. Notably, this is the first crystal structure of a terpenoid cyclase in which a bound substrate analogue adopts a conformation similar to that required

for the precatalytic enzyme-substrate complex. The crystal structures of the ATAS-**3** and ATAS-**4** complexes also provide substantial mechanistic and conformational information. Having previously advanced the idea that aza analogues that are more product-like in structure are more likely to be bound with catalytically-productive orientations[51] based on several crystal structures of terpenoid cyclase-aza analogue complexes,[17,51] we suggest that since **4** is the most product-like of all the aza analogues studied, the corresponding ATAS-**4** complex represents the most catalytically-productive orientation of the bicyclic aza analogue in the ATAS active site. This is consistent with the orientation of the final carbocation intermediate of a terpenoid cyclization being proximal to the PP_i anion, which may play a key role in quenching the final carbocation intermediate (*vide infra*).

Role of active site water in catalysis

The active site of a terpenoid cyclase is generally quite hydrophobic, more complementary in chemical nature to a nonpolar isoprenoid hydrocarbon than to a polar molecule such as water. However, it is intriguing that substrate binding to ATAS does not displace all of the water molecules presumed to solvate the active site in the unliganded enzyme. Trapped water molecule "w" is held firmly in place by hydrogen bonds with N213, N299, and S303 in all structures (Figures 3-8). Since ATAS is a high-fidelity cyclase and there is no evidence for hydroxylated products, this water molecule cannot be acting as a nucleophile. Moreover, a role for this water molecule as a general base is ruled out based on its intermolecular contacts in the ATAS-FSPP complex. Therefore, trapped water molecule "w" simply comprises part of the active site contour, comparable to the trapped water molecule observed in ligand complexes with bornyl diphosphate synthase.[17]

Also interesting is water molecule "ww", which is observed in the ATAS-**3** and ATAS-**5** complexes; however, both **3** and **5** possess incorrect stereochemistry with regard to the ATAS reaction, so we cannot make conclusive mechanistic statements about this water molecule. Since water molecule "ww" is not observed in the ATAS-FSPP complex, the initial assumption would be that it could not enter the active site during catalysis – ostensibly, it only binds when the enzyme is allowed to equilibrate with an aza analogue during the cocrystallization experiment. However, water molecule "ww" is hydrogen bonded to the PP_i anion as well as a Mg^{2+}_C-bound water molecule, which in turn is exposed to bulk solvent. If sufficient void volume were created upon formation of the germacrene A intermediate to open up a new water binding site, this would allow a Mg^{2+}_C-bound water molecule to move into the "ww" position and another water molecule from bulk solvent to move into the vacant coordination site on Mg^{2+}_C. If water molecule "ww" is present during catalysis, it is highly controlled, in that it cannot react with any carbocation intermediates.

Role of the PP_i anion in catalysis

As previously discussed, the PP_i anion appears poised to accept a proton from the cis-C13 methyl group of FPP based on the structure of the ATAS-FSPP complex, consistent with the regiochemistry previously established for this step of the reaction.[40] Since the PP_i anion is a weak base, especially as coordinated to three Mg^{2+} ions, the protonated PP_i anion could serve as the Brønsted acid that protonates the C=C bond at C6 of the reoriented germacrene A intermediate (Figure 1). Although the proton initially abstracted from C13 of FPP is not added back to the substrate,[40,52] this does not rule out the possible role of the protonated PP_i anion as a general acid, provided that exchange of the proton with water is faster than reprotonation of the newly generated germacrene A.

The PP_i anion hydrogen bonds to the same Mg^{2+}_C-bound water molecule in the ATAS-**2**, ATAS-**4**, and ATAS-**5** complexes, as well as the ATAS-PP_i complex;[34] this Mg^{2+}_C-bound water molecule is exposed to bulk solvent. Thus, if the PP_i anion regiospecifically

deprotonates the germacryl cation intermediate from the carbon derived from the cis-C13 methyl group of FPP, and if proton transfer between the conjugate acid of the PP_i anion, the Mg^{2+}_C bound water molecule, and bulk solvent is rapid relative to the rate of C=C bond protonation, then the proton (or deuteron) derived from the cis-C13 methyl group of FPP would exchange with solvent before reprotonation of the germacrene A intermediate. This likely accounts for the fact that the proton initially abstracted from C13 of FPP is not added back to the substrate.[40,52]

In the final step of catalysis, the H-8$_{si}$ proton of the C8 methylene group is oriented toward the PP_i anion, suggesting that the PP_i anion also serves as the general base for the stereospecific deprotonation resulting in formation of (+)-aristolochene. Water molecule "ww" is also located on the same side of analogue **3** as the PP_i anion, so it is possible that water molecule "ww" could function in this role as well. Since water molecule "ww" is not observed in the ATAS-**4** complex, which mimics the putative bound final carbocation intermediate, this may disfavor the role of water molecule "ww" as a proton acceptor. Regardless of whether it is the PP_i anion or water molecule "ww" that accepts the proton from the final carbocation intermediate, this proton is presumably released rapidly into bulk solvent through exchange with the hydrogen bonded Mg^{2+}_C-bound water molecule.

An emerging role for the PP_i anion as a general base general acid-general base in the ATAS mechanism is suggested by the ATAS crystal structures and is consistent with available enzymological measurements. The potential for product-assisted catalysis by the PP_i anion was first suggested by Caruthers and colleagues in the analysis of structure-function relationships in aristolochene synthase from *Penicillium roqueforti*.[53] Subsequently, the structure of FPP synthase from *Escherichia coli* complexed with dimethylallyl-*S*-thiolodiphosphate (DMASPP) and isopentenyl diphosphate similarly implicated the diphosphate group of DMASPP as the stereospecific general base in the chain elongation reaction.[1,54] Recent studies suggest that active site arginine residues that hydrogen bond with the diphosphate group of FPP play an important role in activating the diphosphate leaving group and modulating the chemistry of the diphosphate/PP_i anion in its potential function as a general acid.[55]

Stereochemical discrimination in the ATAS active site

It is surprising that ATAS is capable of binding carbocation analogue **5**, which mimics the incorrect stereoisomer of the product (+)-aristolochene, particularly in view of the fact that ATAS is a high fidelity cyclase – not only does ATAS generate no other cyclic sesquiterpene with an alternative carbon skeleton, but it generates no stereochemical product other than (+)-aristolochene. Such strict product specificity implies that ATAS has evolved to catalytic perfection – in this case, "perfection" does not refer to catalytic efficiency, but instead to the fidelity of the FPP cyclization cascade. A catalytically-perfect cyclase has evolved with an active site contour that serves as a template for the generation of one sole product. While the active site contour of ATAS is quite product-like, i.e., it is complementary in shape to that of (+)-aristolochene, it is remarkable that modest flexibility in the active site accommodates an aristolochene analogue with incorrect stereochemistry.

Transition state binding in an enzyme active site is under kinetic control, with the reaction coordinate from one intermediate to the next being governed by the barrier height separating the intermediates and not the relative binding energies of the intermediates. Thus, the orientation, conformation, and stereochemistry of an analogue designed to mimic a carbocation intermediate allowed to achieve the most favorable binding energy and structure will not necessarily reflect the kinetically-favored structure encountered in catalysis for the corresponding intermediate or transition state. However, the orientations and conformations of stereochemically-correct analogues may become thermodynamically more favorable as

the product structure is approached,[51] and this appears to be the case in the ATAS-**4** complex. Thus, a terpenoid cyclase active site – even that of a high fidelity terpenoid cyclase – may be capable of binding terpenoids and terpenoid analogues with "incorrect" structures and stereochemistries, even though these structures and stereochemistries are not ordinarily encountered under kinetic control during the cyclization cascade. Our future studies will continue to probe these aspects of structural and stereochemical discrimination in terpenoid cyclization reactions catalyzed by ATAS.

Acknowledgments

References

1. Poulter CD, Rilling HC. The prenyl transfer reaction. Enzymic and mechanistic studies of the 1'-4 coupling reaction in the terpene biosynthetic pathway. Acc. Chem. Res. 1978; 11:307–313.

2. Poulter CD. Bioorganic chemistry. A natural reunion of the physical and life sciences. J. Org. Chem. 2009; 74:2631–2645. [PubMed: 19323569]

3. Cane DE. Isoprenoid biosynthesis. Stereochemistry of the cyclization of allylic pyrophosphates. Acc. Chem. Res. 1985; 18:220–226.

4. Cane DE. Enzymatic formation of sesquiterpenes. Chem. Rev. 1990; 90:1089–1103.

5. Wendt KU, Schulz GE. Isoprenoid biosynthesis: manifold chemistry catalyzed by similar enzymes. Structure. 1998; 6:127–133. [PubMed: 9519404]

6. Christianson DW. Structural biology and chemistry of the terpenoid cyclases. Chem. Rev. 2006; 106:3412–3442. [PubMed: 16895335]

7. Christianson DW. Unearthing the roots of the terpenome. Curr. Opin. Chem. Biol. 2008; 12:141–150. [PubMed: 18249199]

8. Allemann RK. Chemical wizardry? The generation of diversity in terpenoid biosynthesis. Pure Appl. Chem. 2008; 80:1791–1798.

9. Degenhardt J, Köllner TG, Gershenzon J. Monoterpene and sesquiterpene synthases and the origin of terpene skeletal diversity in plants. Phytochem. 2009; 70:1621–1637.

10. Aaron JA, Christianson DW. Trinuclear metal clusters in catalysis by terpenoid synthases. Pure Appl. Chem. 2010; 82:1585–1597. [PubMed: 21562622]

11. Miller DJ, Allemann RK. Sesquiterpene synthases: passive catalysts or active players? Nat. Prod. Rep. 2012; 29:60–71. [PubMed: 22068697]

12. Rynkiewicz MJ, Cane DE, Christianson DW. Structure of trichodiene synthase from Fusarium sporotrichioides provides mechanistic inferences on the terpene cyclization cascade. Proc. Natl. Acad. Sci. USA. 2001; 98:13543–13548. [PubMed: 11698643]

13. Proctor RH, Hohn TM. Aristolochene synthase. Isolation, characterization, and bacterial expression of a sesquiterpenoid biosynthetic gene (Ari1) from Penicillium roqueforti. J. Biol. Chem. 1993; 268:4543–4548. [PubMed: 8440737]

14. Felicetti B, Cane DE. Aristolochene synthase: mechanistic analysis of active site residues by site-directed mutagenesis. J. Am. Chem. Soc. 2004; 126:7212–7221. [PubMed: 15186158]

15. Köksal M, Hu H, Coates RM, Peters RJ, Christianson DW. Structure and mechanism of the diterpene cyclase ent-copalyl diphosphate synthase. Nat. Chem. Biol. 2011; 7:431–433. [PubMed: 21602811]

16. Aaron JA, Lin X, Cane DE, Christianson DW. Structure of epi-isozizaene synthase from Streptomyces coelicolor A3(2), a platform for new terpenoid cyclization templates. Biochemistry. 2010; 49:1787–1797. [PubMed: 20131801]

17. Whittington DA, Wise ML, Urbansky M, Coates RM, Croteau RB, Christianson DW. Bornyl diphosphate synthase: Structure and strategy for carbocation manipulation by a terpenoid cyclase. Proc. Natl. Acad. Sci. USA. 2002; 99:15375–15380. [PubMed: 12432096]

18. Faraldos JA, Allemann RK. Inhibition of (+)-aristolochene synthase with iminium salts resembling eudesmane cation. Org. Lett. 2011; 13:1202–1205. [PubMed: 21271717]

19. Faraldos JA, Kariuki B, Allemann RK. Intermediacy of eudesmane cation during catalysis by aristolochene synthase. J. Org. Chem. 2010; 75:1119–1125. [PubMed: 20095558]

20. Ishmuratov GY, Legostaeva YV, Botsman LP, Nasibullina GV, Muslukhov RR, Kazakov DV, Tolstikov GA. Ozonolytic transformations of (S)-(–)-limonene. Russ. J. Org. Chem. 2012; 48:18–24.

21. Takikawa H, Sano S, Mori K. Pheromone synthesis, CLXXXVI. Synthesis of (1S,2R,5R)-bicolorin, the aggregation pheremone of male beech bark beetles (Taphrorychus bicolor), and its (1R,2R,5S) isomer. Eur. J. Org. Chem. 1997; 12:2495–2498.

22. Kido F, Yamaji K, Sinha SC, Abiko T, Kato M. Carbocyclic construction by the [2,3]sigmatropic rearrangement of cyclic sulfonium ylides – a new entry for the stereoselective synthesis of substituted cyclohexanones. Tetrahedron. 1995; 51:7697–7714. 1995.

23. Kedrowski BL. Synthesis of orthogonally protected (R)- and (S)-2-methylcysteine via an enzymatic desymmeterization and Curtius rearrangement. J. Org. Chem. 2003; 68:5403–5406. [PubMed: 12816509]

24. Alsina J, Giralt E, Albericio F. Use of N-tritylamino acids and PyAOP(1) for the suppression of diketopiperazine formation in Fmoc/(t)Bu solid-phase peptide synthesis using alkoxybenzyl ester anchoring linkages. Tetrahedron Lett. 1996; 37:4195–4198.

25. Tehrani KA, D'hooghe M, De Kimpe N. Novel synthesis of indolizidines and quinolizidines. Tetrahedron. 2003; 59:3099–3108.

26. Mehta G, Karmakar S, Chattopadhyay SK. Grob-type fragmentation of a carvone derived β-hydroxymesylate: application to the synthesis of chiral lavandulol derivatives. Tetrahedron. 2004; 2004; 60:5013–5017.

27. Jackman LM, Webb RL, Yick HC. Synthesis and chiroptical properties of some piperidin-2-ones. J. Org. Chem. 1982; 47:1824–1831.

28. Lacroix S, Rixhon V, Marchand-Brynaert J. Synthesis of omega-aminodithioesters. Synthesis. 2006:2327–2334.

29. Guarna A, Lombardi E, Machetti F, Occhiato EG, Scarpi D. Modification of the aza-Robinson annulation for the synthesis of 4-methyl-benzo[c]quinolizin 3 ones, potent inhibitors of steroid 5α-reductase 1. J. Org. Chem. 2000; 65:8093–8095. [PubMed: 11073627]

30. Fernández MF, Söllhuber MM. Synthesis of 5,6,9,10,11,11a-hexahydro-8*H*-naphtho[2,1-α]quinolizine/. Heterocycles. 1987; 26:3059–3063.

31. Otwinowski, Z.; Minor, W. Processing of X-ray diffraction data collected in oscillation mode.. In: Carter, CW., Jr.; Sweet, RM., editors. Methods in Enzymology. Macromolecular Crystallography (Part A). Eds. Vol. 276. Academic Press; New York: 1997. p. 307-326.

32. Karplus PA, Diederichs K. Linking crystallographic model and data quality. Science. 2012; 336:1030–1033. [PubMed: 22628654]

33. McCoy AJ, Grosse-Kunstleve RW, Adams PD, Winn MD, Storoni LC, Read RJ. Phaser crystallographic software. J. Appl. Cryst. 2007; 40:658–674. [PubMed: 19461840]

34. Shishova EY, Di Costanzo L, Cane DE, Christianson DW. X-ray crystal structure of aristolochene synthase from Aspergillus terreus and evolution of templates for the cyclization of farnesyl diphosphate. Biochemistry. 2007; 46:1941–1951. [PubMed: 17261032]

35. Shishova EY, Yu F, Miller DJ, Faraldos JA, Zhao Y, Coates RM, Allemann RK, Cane DE, Christianson DW. X-ray crystallographic studies of substrate binding to aristolochene synthase suggest a metal ion binding sequence for catalysis. J. Biol. Chem. 2008; 283:15431–15439. [PubMed: 18385128]

36. Adams PD, Afonine PV, Bunkoczi G, Chen VB, Davis IW, Echols N, Headd JJ, Hung L-W, Kapral GJ, Grosse-Kunstleve RW, McCoy AJ, Moriarty NW, Oeffner R, Read RJ, Richardson DC, Richardson JS, Terwilliger TC, Zwart PH. PHENIX: a comprehensive Python based system for macromolecular structure solution. Acta Crystallogr., Section D. 2010; 66:213–221. [PubMed: 20124702]

37. Emsley P, Cowtan K. Coot: model-building tools for molecular graphics. Acta Crystallogr., Section D. 2004; 60:2126–2132. [PubMed: 15572765]

38. Chen VB, Arendall WB III, Headd JJ, Keedy DA, Immormino RM, Kapral GJ, Murray LW, Richardson JS, Richardson DC. MolProbity: all atom structure validation for macromolecular crystallography. Acta Crystallogr., Section D. 2010; 66:12–21. [PubMed: 20057044]

39. Cane DE, Prabhakaran PC, Salaski EJ, Harrison PHM, Noguchi H, Rawlings BJ. Aristolochene biosynthesis and enzymatic cyclization of farnesyl pyrophosphate. J. Am. Chem. Soc. 1989; 111:8914–8916.

40. Cane D,E, Prabhakaran PC, Oliver JS, McIlwaine DB. Aristolochene biosynthesis. Stereochemistry of the deprotonation steps in the enzymatic cyclization of farnesyl pyrophosphate. J. Am. Chem. Soc. 1990; 112:3209–3210.

41. Calvert MJ, Ashton PR, Allemann RK. Germacrene A is a product of the aristolochene synthase mediated conversion of farnesylpyrophosphate to aristolochene. J. Am. Chem. Soc. 2002; 124:11636–11641. [PubMed: 12296728]

42. Dougherty DA. Cation-π interactions in chemistry and biology: a new view of benzene, Phe, Tyr, and Trp. Science. 1996; 271:163–168. [PubMed: 8539615]

43. Dougherty DA. The cation-π interaction. Acc. Chem. Res. 2013; 46:885–893. [PubMed: 23214924]

44. Faraldos JA, Antonczak AK, González V, Fullerton R, Tippmann EM, Allemann RK. Probing eudesmane cation-π interactions in catalysis by aristolochene synthase with non canonical amino acids. J. Am. Chem. Soc. 2011; 133:13906–13909. [PubMed: 21815676]

45. Lesburg CA, Zhai G, Cane DE, Christianson DW. Crystal structure of pentalenene synthase: mechanistic insights on terpenoid cyclization reactions in biology. Science. 1997; 277:1820–1824. [PubMed: 9295272]

46. Starks CM, Back K, Chappell J, Noel JP. Structural basis for cyclic terpene biosynthesis by tobacco 5-epi-aristolochene synthase. Science. 1997; 277:1815–1820. [PubMed: 9295271]

47. Wendt KU, Poralla K, Schulz GE. Structure and function of a squalene cyclase. Science. 1997; 277:1811–1815. [PubMed: 9295270]

48. Deligeorgopoulou A, Allemann RK. Evidence for differential folding of farnesyl pyrophosphate in the active site of aristolochene synthase: a single-point mutation converts aristolochene synthase into an (E)-β-farnesene synthase. Biochemistry. 2003; 42:7741–7747. [PubMed: 12820883]

49. Calvert MJ, Taylor SE, Allemann RK. Tyrosine 92 of aristolochene synthase directs cyclisation of farnesyl pyrophosphate. Chem. Commun. 2002:2384–2385.

50. Gennadios HA, González V, Di Costanzo L, Li A, Yu F, Miller DJ, Allemann RK, Christianson DW. Crystal structure of (+)-δ-cadinene synthase from Gossypium arboreum and evolutionary divergence of metal binding motifs for catalysis. Biochemistry. 2009; 48:6175–6183. [PubMed: 19489610]

51. Vedula LS, Rynkiewicz MJ, Pyun H-J, Coates RM, Cane DE, Christianson DW. Molecular recognition of the substrate diphosphate group governs product diversity in trichodiene synthase mutants. Biochemistry. 2005; 44:6153–6163. [PubMed: 15835903]

52. Miller DJ, Gao J, Truhlar DG, Young NJ, González V, Allemann RK. Stereochemistry of eudesmane cation formation during catalysis by aristolochene synthase from Penicillium roqueforti. Org. Biomol. Chem. 2008; 6:2346–2354. [PubMed: 18563268]

53. Caruthers JM, Kang I, Rynkiewicz MJ, Cane DE, Christianson DW. Crystal structure determination of aristolochene synthase from the blue cheese mold, Penicillium roqueforti. J. Biol. Chem. 2000; 275:25533–25539. [PubMed: 10825154]

54. Hosfield DJ, Zhang Y, Dougan DR, Broun A, Tari LW, Swanson RV, Finn J. Structural basis for bisphosphonate mediated inhibition of isoprenoid biosynthesis. J. Biol. Chem. 2004; 279:8526–8529. [PubMed: 14672944]

55. Faraldos JA, González V, Allemann RK. The role of aristolochene synthase in diphosphate activation. Chem. Commun. 2012; 48:3230–3232.
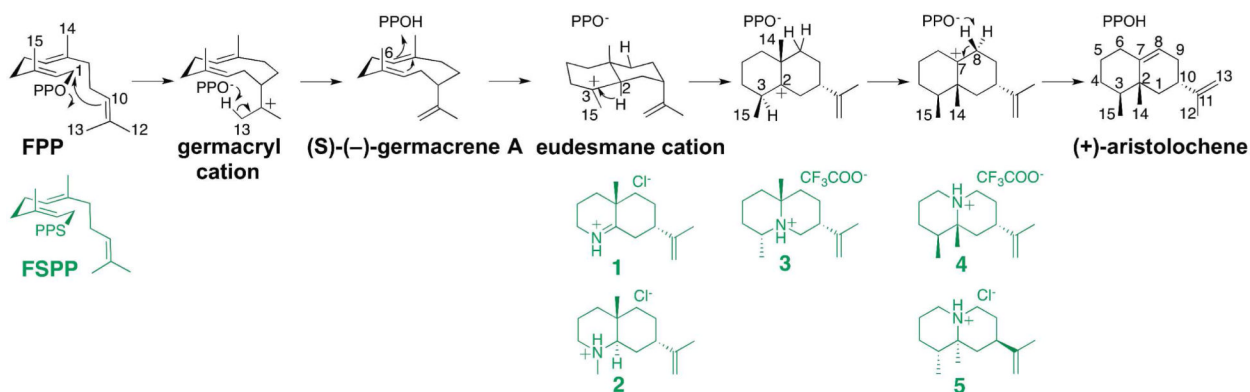
Figure 1.
Proposed mechanism of (+)-aristolochene generation as catalyzed by *A. terreus* aristolochene synthase (PPO = diphosphate; PPO⁻ = inorganic pyrophosphate; PPOH = protonated inorganic pyrophosphate). Note that the germacrene A intermediate must reorient itself relative to protonated inorganic pyrophosphate (which is rigidly positioned by metal coordination and hydrogen bond interactions) to enable subsequent protonation and deprotonation steps in catalysis. Certain sequences might proceed in concerted rather than stepwise fashion, in which case carbon atoms bearing full positive charges would only develop partial positive charges. Carbon atoms are numbered in all structures based on the numbering scheme shown for FPP to better follow relevant carbon atoms during the course of the reaction. Analogues of substrate and possible carbocation intermediates in the cyclization cascade are shown in green.
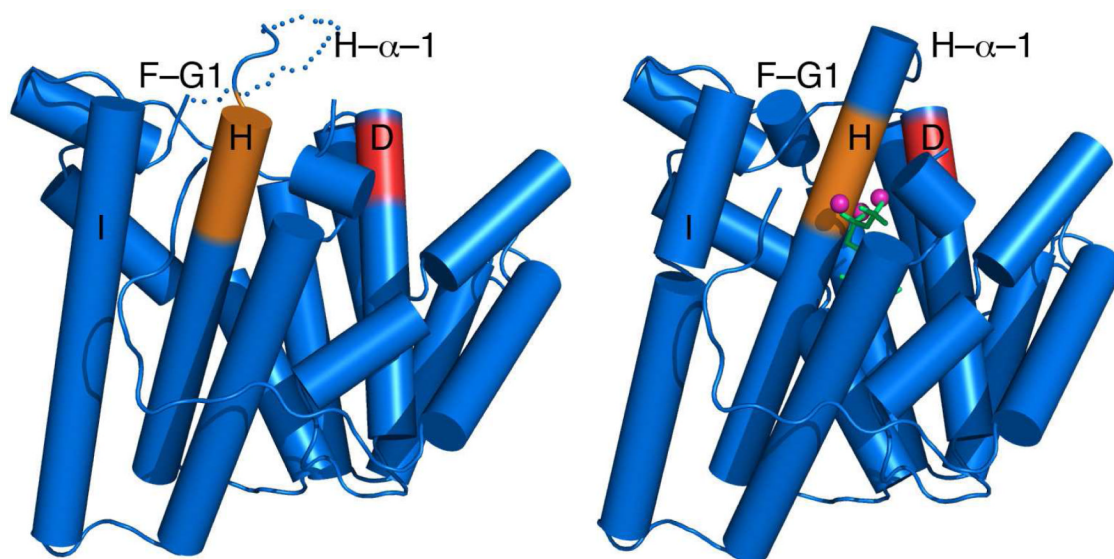
Figure 2.
Structural comparison of unliganded ATAS (left) with the ATAS-FSPP complex (right) illustrating conformational changes triggered by the binding of FSPP and 3 Mg^{2+} ions in the active site. The aspartate-rich DDXXD metal-binding segment on helix D is red and the "NSE" metal-binding segment on helix H is orange. In the ATAS-FSPP complex, Mg^{2+} ions are magenta and FSPP is shown as a stick-figure. Selected secondary structure elements are labeled as discussed in the text.
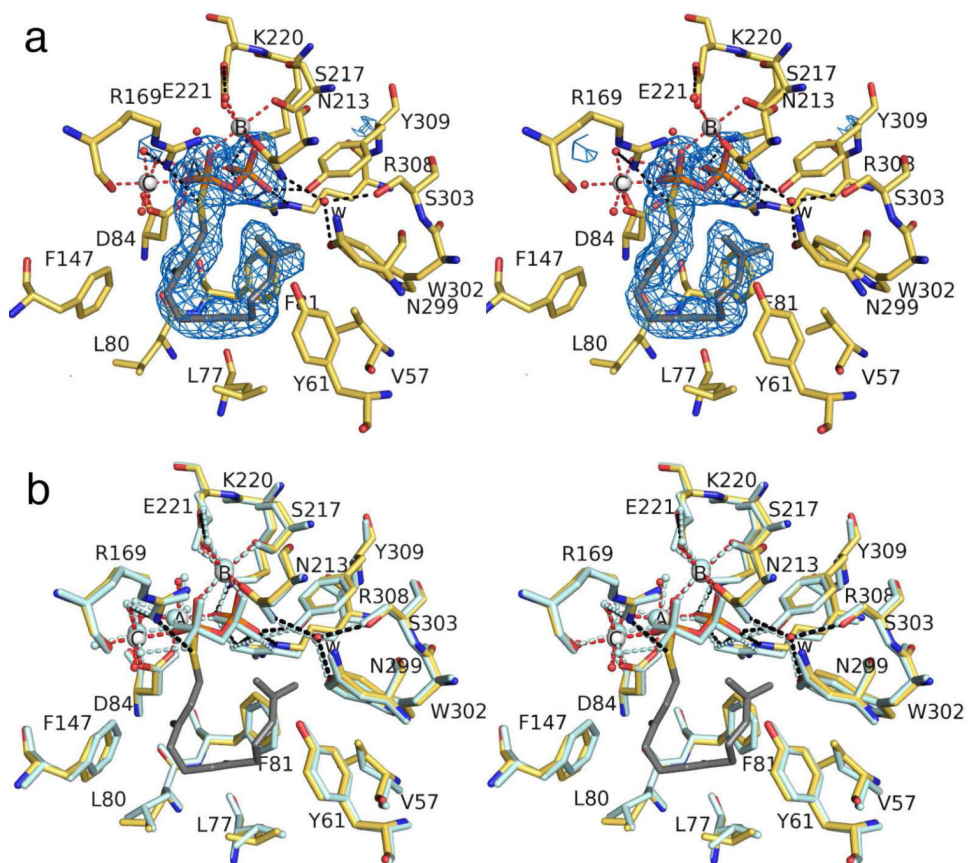
Figure 3.
(a) Simulated annealing omit map of FSPP (contoured at 4.0σ) bound to monomer A in the ATAS-Mg^{2+}_3-FSPP complex. Atoms are color-coded as follows: C = yellow (protein) or gray (FSPP), O = red, N = blue, P = orange, S = yellow, Mg^{2+} ions = silver spheres, solvent molecules = red spheres. Metal coordination interactions are shown as red dotted lines; hydrogen bond interactions are shown as black dotted lines. Water molecule "w" is trapped in the active site along with FSPP. (b) Superposition of the ATAS-Mg^{2+}_3-FSPP complex (color-coded as in (a)) and the ATAS-Mg^{2+}_3-PP_i complex (all atoms pale cyan).
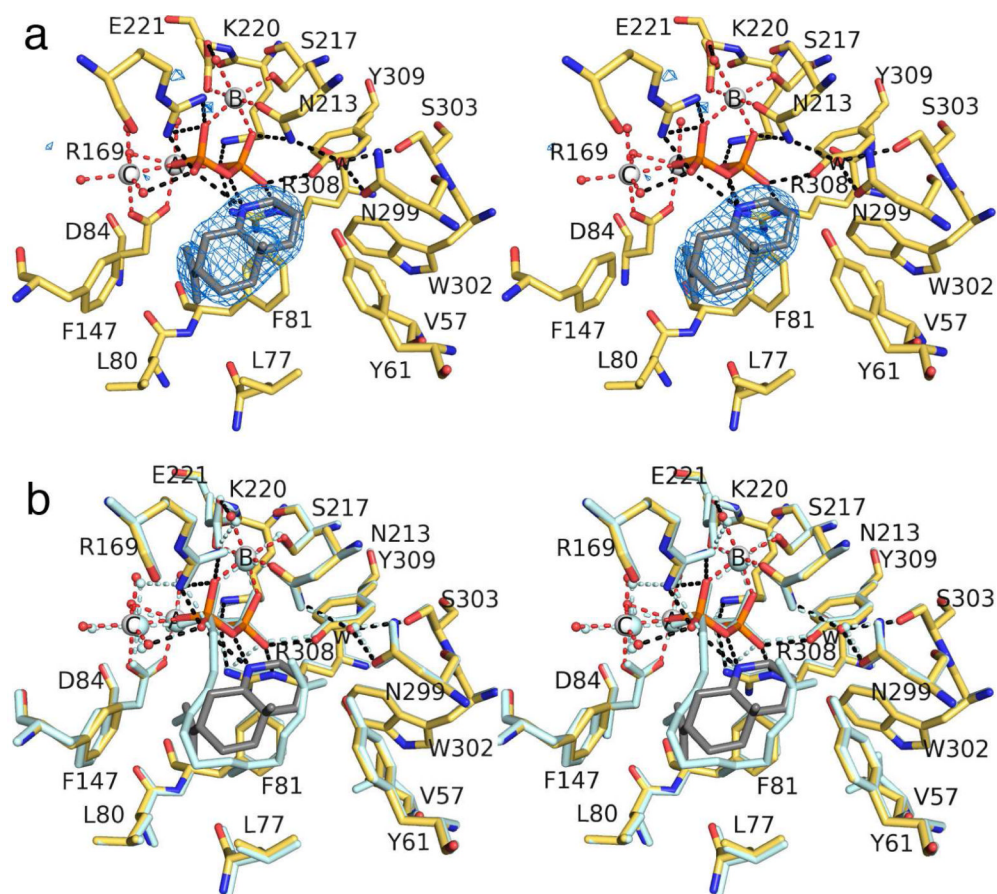
Figure 4.
(a) Simulated annealing omit map of iminium cation **1** (contoured at 4.0σ) bound to monomer A in the ATAS-**1** complex. Atoms are color-coded as follows: C = yellow (protein) or gray (**1**), O = red, N = blue, P = orange, S = yellow, Mg^{2+} ions = silver spheres, solvent molecules = red spheres. Metal coordination and hydrogen bond interactions are shown as red and black dotted lines, respectively. Water molecule "w" is trapped in the active site along with **1**. (b) Superposition of the ATAS-**1** complex (color-coded as in (a)) and the ATAS-FSPP complex (all atoms pale cyan).
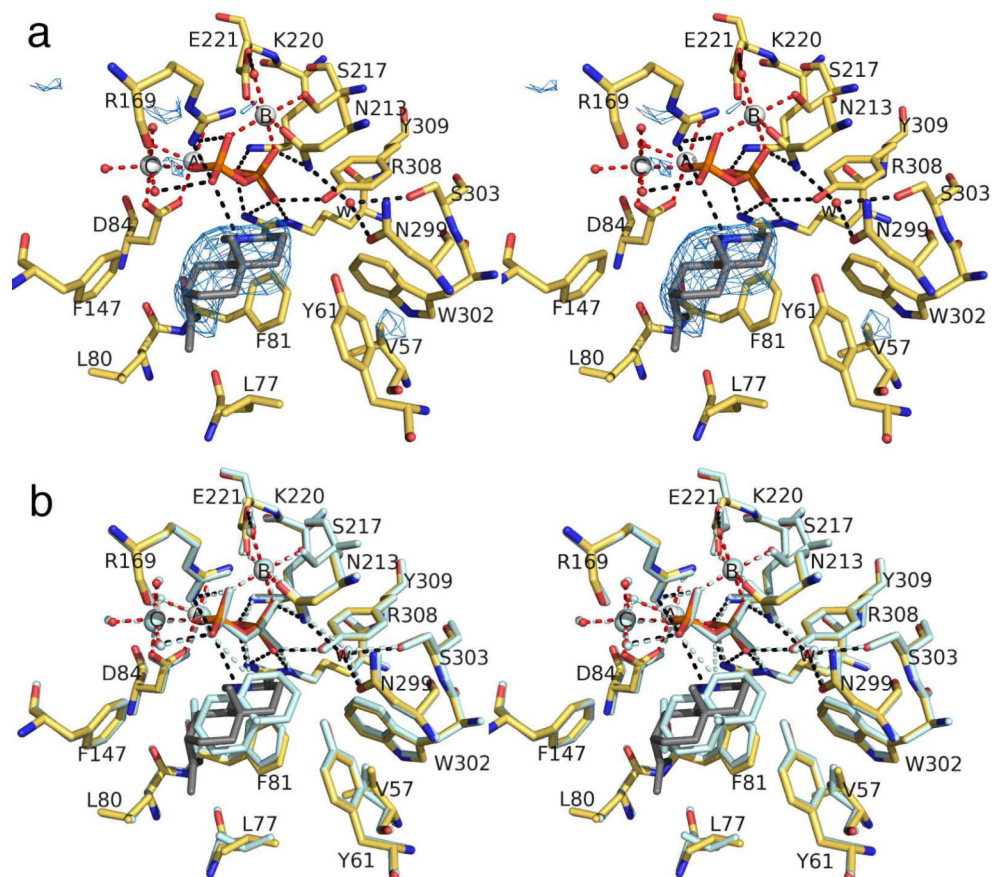
Figure 5.
(a) Simulated annealing omit map of tertiary ammonium cation **2** (contoured at 2.6σ) bound to monomer A in the ATAS-**2** complex. Atoms are color coded as follows: C = yellow (protein) or gray (**2**), O = red, N = blue, P = orange, S = yellow, Mg^{2+} ions = silver spheres, solvent molecules = red spheres. Metal coordination and hydrogen bond interactions are shown as red and black dotted lines, respectively. Water molecule "w" is trapped in the active site along with **3**. (b) Superposition of the ATAS-**2** complex (color coded as in (a)) with the ATAS-**1** complex (all atoms pale cyan).
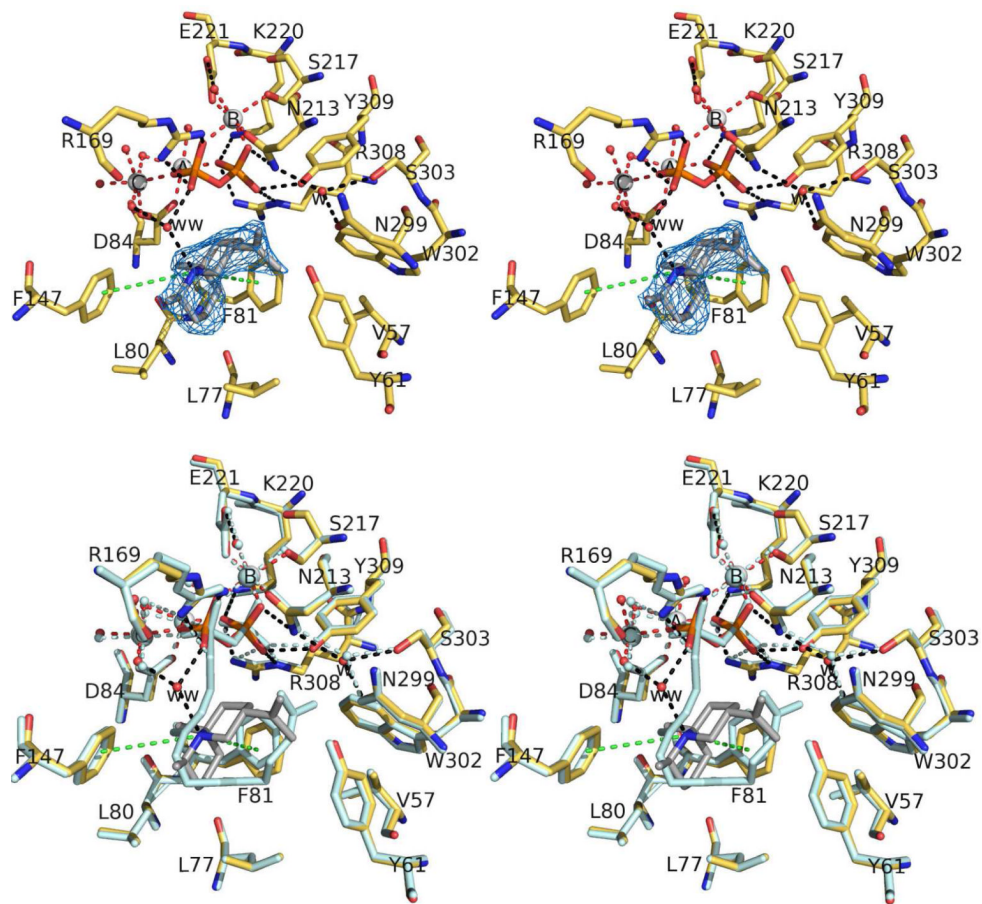
Figure 6.
(a) Simulated annealing omit map of tertiary ammonium cation **3** (contoured at 3.5σ) bound to monomer B in the ATAS-**3** complex. Atoms are color coded as follows: C = yellow (protein) or gray (**3**), O = red, N = blue, P = orange, S = yellow, Mg^{2+} ions = silver spheres, solvent molecules = red spheres. Metal coordination, hydrogen bond, and cation-π interactions are shown as red, black, and green dotted lines, respectively. Water molecules "w" and "ww" are trapped in the active site along with **3**. (b) Superposition of the ATAS-**3** complex (color coded as in (a)) with the ATAS-FSPP complex (all atoms pale cyan).

Figure 7.
(a) Simulated annealing omit map of tertiary ammonium cation **4** (contoured at 3.0σ) bound to monomer A in the ATAS-**4** complex. Atoms are color-coded as follows: C = yellow (protein) or gray (**4**), O = red, N = blue, P = orange, S = yellow, Mg^{2+} ions = silver spheres, solvent molecules = red spheres. Metal coordination, hydrogen bond, and cation-π interactions are shown as red, black, and green dotted lines, respectively. Water molecule "w" is trapped in the active site along with **4**. (b) Superposition of the ATAS-**4** complex (color coded as in (a)) with the ATAS-FSPP complex (all atoms pale cyan).
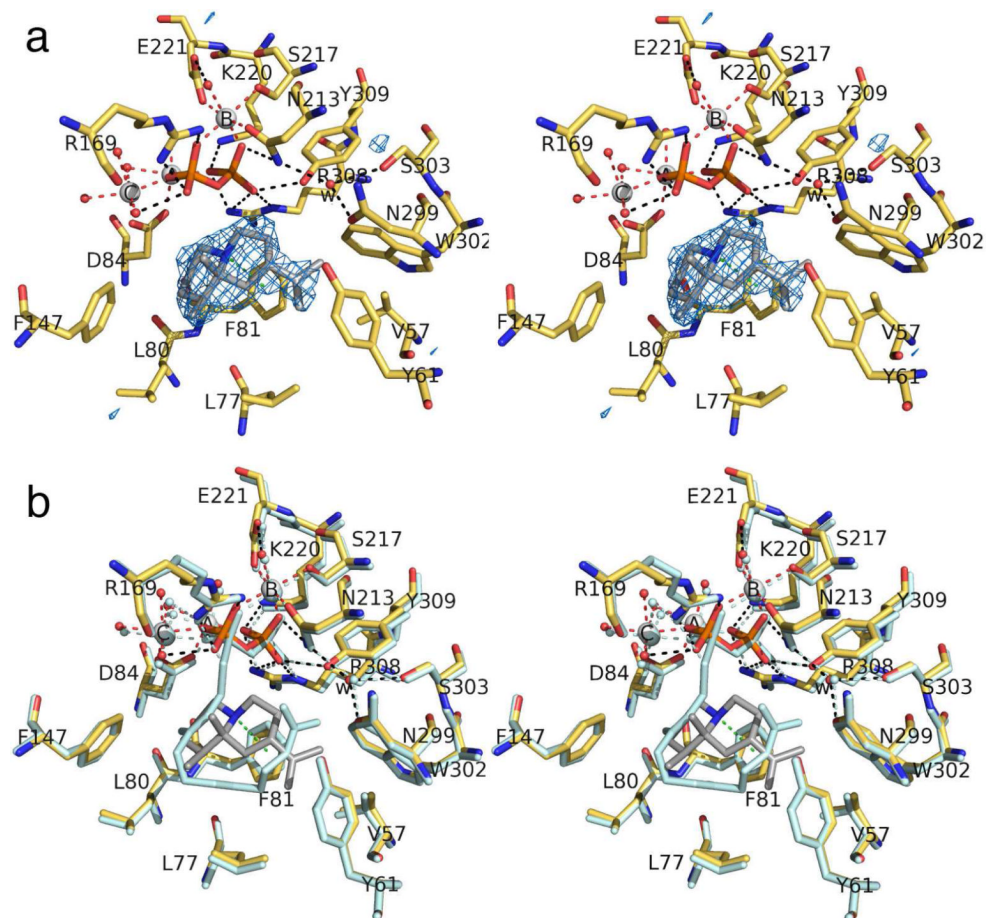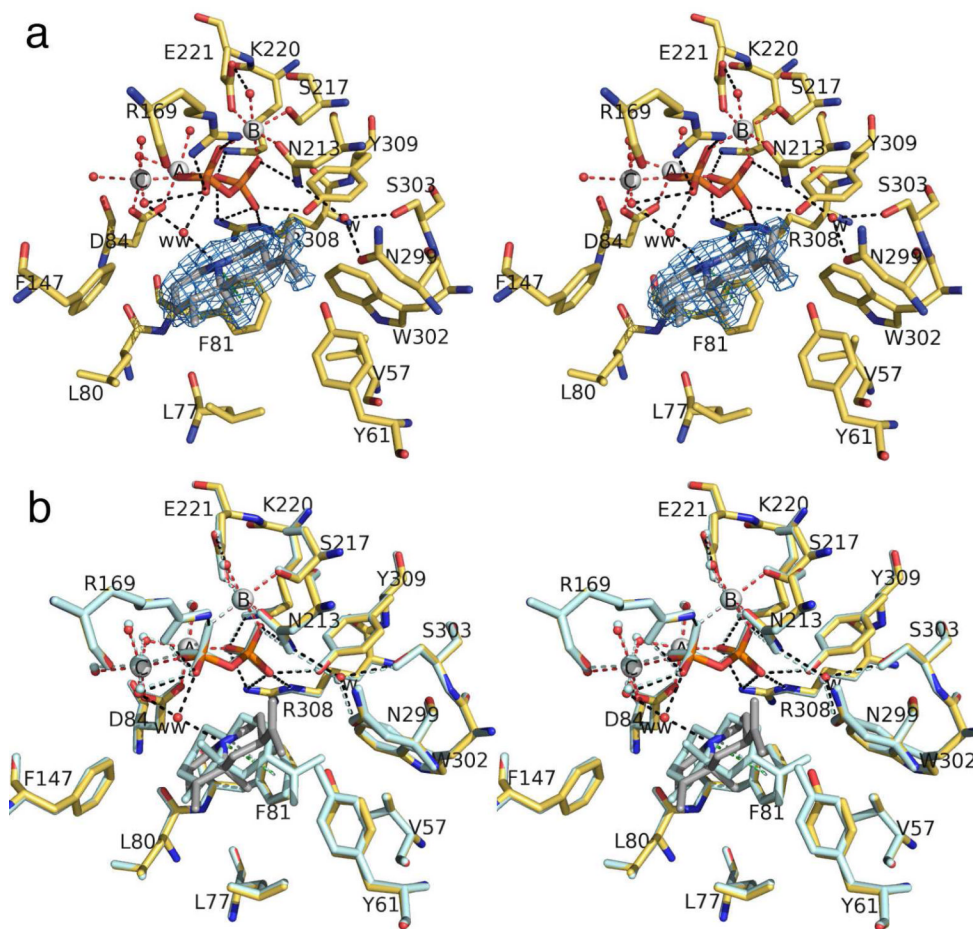
Figure 8.
(a) Simulated annealing omit map of tertiary ammonium cation **5** (contoured at 3.1σ) bound to monomer A in the ATAS-**5** complex. Atoms are color coded as follows: C = yellow (protein) or gray (**5**), O = red, N = blue, P = orange, S = yellow, Mg^{2+} ions = silver spheres, solvent molecules = red spheres. Metal coordination, hydrogen bond, and cation-π interactions are shown as red, black, and green dotted lines, respectively. Water molecules "w" and "ww" are trapped in the active site along with **5**. (b) Superposition of the ATAS-**5** complex (color coded as in (a)) with the ATAS-**4** complex (all atoms pale cyan).

Table 1

Data collection and refinement statistics

Complex	ATAS-FSPP	ATAS-1	ATAS-2	ATAS-3	ATAS-4	ATAS-5
A. Data Collection						
Resolution limits (Å)	50.0-1.90	50.0-2.15	50.0-2.40	50.0-2.10	50.0-1.95	50.0-1.86
Total/unique reflections measured	1605556/142524	537459/96119	783788/69718	1104453/105878	965747/130854	1034908/151303
Space group	$P3_121$	$P3_121$	$P3_121$	$P3_121$	$P3_121$	$P3_121$
Unit cell: a, c (Å)	124.0, 203.5	123.4, 201.6	122.8, 202.5	124.4, 202.9	124.3, 203.0	123.8, 202.1
R_{merge} [a,b]	0.102 (*)	0.106 (0.569)	0.094 (0.277)	0.127 (0.702)	0.132 (0.681)	0.102 (0.763)
$I/\sigma(I)$ [a]	30.4 (1.5)	16.3 (3.2)	30.0 (9.3)	19.3 (3.4)	14.1 (3.3)	17.5 (2.8)
Redundancy [a]	11.3 (10.9)	5.6 (5.6)	11.2 (9.4)	10.4 (9.9)	7.4 (7.3)	6.8 (6.6)
Completeness (%) [a]	100.0 (100.0)	99.1 (99.9)	100 (100)	100.0 (100.0)	99.4 (98.8)	100 (100)
B. Refinement						
Reflections used in Refinement/ test set	142431/7147	96109/4811	69619/3517	105808/5287	130821/6591	150235/7536
R_{work} [c]	0.189	0.208	0.174	0.194	0.191	0.193
R_{free} [c]	0.226	0.240	0.212	0.229	0.238	0.226
Protein atoms [d]	9831	9816	9816	9839	9831	9831
Ligand atoms [d]	96	92	96	96	96	96
Mg^{2+} ions [d]	12	12	13	12	12	12
Solvent atoms [d]	978	892	980	980	1077	1024
Glycerol atoms [d]	12	0	24	12	6	12
Avg. B factors (Å²)						
main chain	32	19	26	29	26	24
side chain	37	22	28	32	30	28
ligand	33	13	35	31	29	26
Mg^{2+} ions	27	16	23	23	22	18
solvent	37	27	30	35	31	29
R.m.s. deviations						
bonds (Å)	0.014	0.005	0.005	0.005	0.007	0.016
angles (deg)	1.4	0.8	0.8	0.8	1.0	1.5
Ramachandran Plot (%)						
Allowed	95.1	95.3	94.8	95.0	95.5	95.2
Additionally allowed	4.9	4.7	5.2	5.0	4.5	4.8
Generously allowed	0.0	0.0	0.0	0.0	0.0	0.0
disallowed	0.0	0.0	0.0	0.0	0.0	0.0
PDB accession code	4KUX	4KVI	4KVD	4KVW	4KVY	4KWD

[a]Numbers in parentheses refer to the highest resolution shell of data.

[b]R_{merge} for replicate reflections, $R = \Sigma |I_h - \langle I_h \rangle| / \Sigma \langle I_h \rangle$; I_h = intensity measure for reflection h; and $\langle I_h \rangle$ = average intensity for reflection h calculated from replicate data.

[c]$R_{work} = \Sigma \|F_O| - |F_c\| / \Sigma |F_O|$ for reflections contained in the working set. $R_{free} = \Sigma \|F_O| - |F_c\| / \Sigma |F_O|$ for reflections contained in the test set held aside during refinement (5% of total). $|F_O|$ and $|F_c|$ are the observed and calculated structure factor amplitudes, respectively.

[d]Per asymmetric unit.

[*]R_{merge} value higher than 1.000 are reported as 0.000 by HKL2000. Given the exceptionally high redundancy of 10.9 for the outer shell of this dataset, R_{pim} is a more appropriate measure of data quality than R_{merge}. For this dataset, $R_{pim} = 0.037$ (0.572).